Laboratory Study on the Behavior of a Horizontal Ellipse Culvert during Service and Ultimate Load Testing

Caleb Regier[1], Neil A. Hoult, M.ASCE[2], and Ian D. Moore, M.ASCE[3]

Abstract: Horizontal ellipse culverts have been used for many years as a substitute for more conventional short span bridges, however their performance has never been evaluated experimentally. This paper describes an experimental program to understand the behavior of a horizontal ellipse culvert during backfilling, when subjected to simulated service loading at the ground surface, and during an ultimate limit states test. The backfill response of the specimen was similar to circular culverts except that, as expected, the specimen exhibited lower vertical stiffness as compared to its horizontal stiffness due to its shape. Contrary to current design conventions, the response of the culvert to surface loading was influenced by the cover depth. At 0.9 m of cover, the load carrying mechanism was ring compression, whereas at 0.45 m significant bending stresses developed in the top of the pipe. The ultimate capacity of the culvert was measured at 0.45m of

[1] Researcher, GeoEngineering Centre at Queen`s - RMC, Queen's University, Kingston, On., Canada, K7L 3N6. E-mail: caleb.regier@gmail.com
[2] Associate Professor, Department of Civil Engineering, Queen's University, Ellis Hall, Kingston, On., Canada, K7L 3N6. E-mail: neil.hoult@gmail.com
[3] Professor and Canada Research Chair in Infrastructure Engineering, GeoEngineering Centre at Queen`s - RMC, Queen`s University, Kingston, Ontario, Canada, K7L 3N6. E-mail: ian.moore@queensu.ca

cover to be a tandem axle load of 1324 kN. While this is approximately twice the fully factored design load, the culvert failed after the development of a plastic hinge mechanism instead of the wall compression considered in the AASHTO and Canadian design codes, though the structure still had reserve capacity.

CE Database subject headings: Culverts; Laboratory tests; Soil-pipe interactions; Steel; Strain distribution

Introduction

The use of soil-steel structures as substitutes for the more conventional types of bridges, especially short span bridges, has grown rapidly since they were developed in the 1960s (Mirza and Porter, 1981). The 1960s were a decade of intense research on soil-steel structures, which was prompted by the acceptance of ring compression theory (White and Layer, 1960). Following this acceptance, hundreds and thousands of culverts were installed across North America, as these structures were shown to provide a cost effective alternative for short span bridges. Since the failure of a metal culvert can have significant adverse effects, it is fundamental for bridge engineers to understand how each culvert behaves when subjected to earth and vehicle loads. According to the Handbook of Steel Drainage & Highway Construction Products (CSPI, 2009) as well as the American (AASHTO, 2007), and Canadian bridge design codes (CSA, 2014), steel culverts are currently designed considering compression failures due to wall crushing or buckling. While the flexural response of large span corrugated metal culverts was investigated by Duncan and his collaborators in the 1970s and 1980s (Duncan, 1978; Duncan et al.,1985), potential failure modes such as local bending moments and the development of plastic hinges are usually not considered for small diameter circular and elliptical pipes. However, no laboratory

based experimental testing has been undertaken to evaluate these design assumptions for the horizontal ellipse.

A number of studies have been conducted on the stability of circular culverts (e.g. Seed & Raines, 1988; Taleb & Moore, 1999; El-Sawy, 2003; Moore, 2012; Mai et al., 2013; Elshimi et al., 2014), however the behavior of horizontal ellipse culverts is less well understood. Currently there is limited information available regarding the load carrying capacity of horizontal ellipse culverts, with no test ever reported where one of these structures has been loaded up to its ultimate limit state.

Moore (1988a; 1988b) performed a parametric study using finite element analysis on the static response and buckling of elliptical tubes deeply buried within uniform elastic soil to determine their structural response. The study developed a procedure for estimating the distribution of resultants and radial deformations around buried elliptical tubes ranging from high to low stiffness. Moore et al. (1995) conducted an investigation on 39 corrugated steel plate culverts in the field in an effort to create a method for reviewing the conditions of long span corrugated steel culverts. The investigation included a range of culvert spans, heights, and shapes including multiple horizontal ellipses. However, neither of these studies involved load testing of a horizontal ellipse culvert to failure.

The objectives of this research program are to (i) investigate the behavior of a horizontal ellipse culvert during backfill, (ii) examine the failure mode of a horizontal ellipse culvert and, (iii) assess the overall structural stability of this type of culvert. This paper describes the burial and behavior of a horizontal ellipse culvert tested under a simulated surface load. The first section of this paper introduces the experimental background including backfill, specimen

63 sectional properties, instrumentation and the applied loading procedure. The results of the
64 experiment will then be presented and discussed followed by key conclusions.

65

66 **Design of Culverts**

67 In order to compare the experimental results to the expected performance of the culvert,
68 calculations of loading (demand) and capacity (resistance) are now provided. Culvert design is
69 covered by the American Association of State Highway and Transportation Officials (AASHTO)
70 LRFD Bridge Design Specifications (SI) (AASHTO, 2007) as well as the Canadian Highway
71 Bridge Design code (CSA, 2014). The AASHTO design provisions require that the culvert be
72 checked against the maximum thrust force per unit length, T_L in N/mm, calculated using equation
73 1.

74 $$T_L = \frac{P_L(S)}{2} \quad (1)$$

75 P_L is the factored crown pressure (MPa), and S is the span of the culvert (mm).

76 The Canadian code (CSA, 2014) indicates that soil-metal structures with shallow
77 corrugations need to be designed against compression failure under regular vehicle traffic, a plastic
78 hinge forming during construction, and connection failures (though culvert design according to the
79 Canadian code is only required for structures with spans of at least 3m, it has been employed here
80 for the somewhat smaller test culvert). For compression failure, the thrust force, T_f, in the culvert
81 wall is given by equation 2 in units of kN/m.

82 $$T_f = \alpha_D T_D + \alpha_L T_L(1 + DLA) \quad (2)$$

The thrust force due to dead load, T_D, (kN/m), the thrust force due to live load, T_L (kN/m), and the dynamic load allowance are given by equations 3, 4, and 5, respectively. The dead and live load factors, α_D and α_L, will be set to unity in this analysis.

$$T_D = 0.5(1.0 - 0.1C_s)A_f W \quad (3)$$

C_s is the axial stiffness taken as $1000E_sD_v/EA$, A_f is a factor accounting for the shape of the culvert and the height of the soil cover determined from a figure given in the code, and W is the weight of the soil above the culvert (including the soil above the shoulders) in kN/m. Additionally, E_s is the secant modulus of the soil based on soil type and density in MPa, D_v is the vertical diameter of the culvert in m, and EA is the axial stiffness of the culvert in N/mm.

$$T_L = 0.5D_h\sigma_L m_f = 0.5l_t\sigma_L m_f \quad (4)$$

D_h is the horizontal diameter of the culvert (m), σ_L is the equivalent dispersed unfactored live load at the crown (kPa), m_f is the multi-lance loading factor (set to unity in this analysis), and l_t is the distance between the outermost axles including tire footprints (m).

$$TLA = 0.40(1 - 0.5D_E) \geq 0.1 \quad (5)$$

D_E is the earth cover above the culvert.

To determine if a plastic hinge will form in the culvert during construction, the unfactored thrust force, P in kN/m, is calculated using equation (6) while the unfactored bending moment, M in kNm/m, is calculated using equation (7).

$$P = T_D + T_C \quad (6)$$

T_D is calculated using equation 6 and T_C is calculated using equation 7 but with construction lives loads.

$$M = M_1 + M_B + M_C \quad (7)$$

M_1 is the moment resulting from fill to the crown (kNm/m), M_B is the moment resulting from fill above the crown (kNm/m), and M_C is the additional moment due to construction live loads (kNm/m), all of which are specified in the code (CSA, 2014) and are not given here for the sake of brevity. For the current analysis the loads applied during the experiment will be considered construction loads when using equations 6 and 7.

Experimental background

The culvert was tested under different cover depths (height of soil above the crown of the pipe) and to different load levels. There were four tests in total: (i) a response to burial under 0.9 m of soil test, (ii) a maximum service load test at 0.9 m of cover, (iii) a maximum service load test at 0.45 m of cover, and (iv) an ultimate limit state (ULS) test at 0.45 m of cover. The culvert was tested using a frame with geometry equivalent to a tandem axle and a 2000 kN load actuator to apply vertical forces that represent vehicular surface loading over the buried metal culvert. The culvert was buried in well compacted granular soil in the 8 m long, 8 m wide and 3 m deep reinforced concrete test pit described by Moore (2012). During the surface load testing, the load was applied in multiple cycles in order to simulate first loading as well as repeated loading conditions.

Test configuration

The culvert was placed on a loose bedding material in a North-South oriented trench centered within the concrete pit such that the invert (the bottom of the pipe) of the culvert rested

at the base of the trench as illustrated in Fig. 1(a). The trench sidewalls were 1.1 m away from the sides of the pipe on both sides prior to burial. The specimen was placed in the test pit such that the concrete walls of the test pit were 3.20 m from the sides of the culvert specimen.

Upon the completion of backfilling, a 2000 kN hydraulic actuator was attached to the stiff frame above the test pit, such that it was centered along the culvert specimen as shown in Fig. 1(b) and Fig. 2(a) and (b). The load was transmitted from the actuator to four steel pads (described subsequently) on the soil surface.

Experimental specimen

The ellipse had a span of 1.6 m, rise of 1.35 m and length of 6.5 m. The corrugation amplitude was 25.4 mm with a period of 76.2 mm and a wall (steel plate) thickness of 1.82 mm. The corrugated steel plate had an area of A = 2.259 mm^2/mm, and a second moment of area of I = 170.40 mm^4/mm, as reported by the CSPI (2009). As specified by ASTM A796 (2015), the steel had an assumed minimum yield strength (f_y) of 230 MPa, a minimum tensile strength (f_u) of 310 MPa and a Young's modulus of 200,000 MPa. The yield strain, 1150 με, of the culvert was calculated by dividing the minimum yield strength by the Young's modulus. The compressive thrust which induces yield in the culvert's wall was 520 kN/m, as calculated by multiplying the cross sectional area per meter by the minimum yield strength. The bending moment required to produce initial yielding at the extreme fiber in the absence of axial load was calculated to be 2.84 kNm/m using the section properties of the corrugated plate. The presence of axial force at the same cross section as the peak moment will reduce the moment required to cause the steel to yield at that location.

Backfill

The specimen was backfilled with poorly-graded sandy gravel (classified as “GP-SP” using the unified soil classification system). The soil grading for the test soil is reported by Lougheed (2008). The bedding material for each culvert was compacted using a vibrating plate tamper (Wacker wp1550AW) to 95% standard Proctor (95% of the maximum dry unit weight achieved using a Standard Proctor test) as measured by a model MC1DR-P nuclear densometer. Soil was added in 300 mm lifts and compacted to 90% standard Proctor from the invert to the crown using the same vibrating plate tamper. The soil beneath the haunch (the area midway between the bottom and the side) of the culvert was compacted using foot tamping in an effort to achieve 90% standard Proctor compaction beneath the haunch. At the end of each lift, the dry density, water content, percentage of Standard Proctor and the height were all recorded. From the crown to the top of cover (0.9 m and 0.45 m depending on the test configuration) the soil was compacted to 95 % standard Proctor, once again adding soil in 300 mm lifts. A summary of the soil properties is provided in Table 1.

Loading

Surface live load was applied using a simulated tandem axle configuration. Tandem axle loading was chosen as the most critical loading scenario (as compared to loads applied to a single axle or single wheel pad). The tandem axle used had a geometry of 1.2 m by 1.8 m center to center, in accordance with the tandem axle geometry for the CL-625-(ONT) design truck (CSA, 2014).

For the service load tests, the load was applied to the surface through steel plates designed to simulate Canadian standard wheel pairs measuring 250 mm by 600 mm. At 0.9 m of cover, the full service load of 323 kN for the American bridge design code (AASHTO, 2007) and 342 kN for the Canadian bridge design code (CSA, 2014) was applied. The load was cycled between zero and the full service load three times to measure the behavior under initial and repeated loading. At 0.45 m of cover the specimen was again loaded to the full service load of 338 kN (AASHTO, 2010) and 367 kN (CSA, 2014) using three load cycles.

The specimen was then loaded to its ultimate limit states load at 0.45 m of cover. To prevent premature bearing failure of the soil at the surface from being the ultimate limit state, enlarged wooden wheel pads (950 mm long by 370 mm wide) were used for this test. In all cases the load was applied at a loading rate of 50 kN/min.

Instrumentation

The vertical (denoted V in figures) and horizontal (denoted H in figures) diameter change of the culvert was measured using linear potentiometers as shown in Fig. 3. A total of 4 linear potentiometers were installed, two directly beneath the actuator and two offset by 0.9 m to the North of the actuator (located directly under the North tandem axle wheel pads). From here on, the location directly below the actuator is referred to as the Center location, and the location offset 0.9 m North of the actuator is referred to as the North location.

A camera was set up just outside the culvert to take pictures of the culvert looking along its longitudinal axis for use with Digital Image Correlation (DIC). DIC allows the movement of regions of interest in a series of digital images to be tracked (Take, 2015) and in this case was used

192 to evaluate the deformation of the culvert during the test. A series of targets were glued to the
193 culvert around the circumference as seen in Fig. 3. The images for the DIC analysis were taken
194 every 30 seconds during loading using a Canon T3i DSLR camera. The targets around the
195 circumference were tracked in the image series and the deformations were determined using the
196 Matlab based DIC program called GeoPIV (Take, 2015).

197 Previous work by Simpson et al. (2015) showed that distributed fiber optic strain sensors
198 based on Rayleigh backscatter provided distributed strains around the circumference of the pipe
199 with similar accuracy to conventional electrical resistance strain gauges. As such, four fiber optic
200 cables were installed on the interior corrugations of the culvert specimen to enable strain
201 measurements to be taken at each load step as illustrated in Fig. 3. A nylon coated fiber was
202 installed both in the valley and crest of both corrugations monitored (Center and North location).
203 Installation details for the nylon fibers on steel are discussed by Simpson et al. (2015). The
204 distributed strain measurements were taken with a gauge length of 20 mm at a sensor spacing of
205 20 mm using a Luna OBR 4600 fiber optic strain analyzer.

206

207 **Resultant thrusts and bending moments**

208 The thrust forces and bending moments that are discussed in the Results section were
209 calculated from strains obtained from the fiber optic sensors. The strains on the ellipse were
210 measured on the inside corrugation valley (the steel fiber closest to the longitudinal axis of the
211 culvert), ε_1, and the inside corrugation crest (the steel fiber farthest from the longitudinal axis of
212 the culvert but still inside the pipe), ε_2. As the crest sensors were not installed at the extreme
213 fiber location, the exterior crest strain (extreme fiber strain) was estimated using linear

extrapolation. The average strain (ε_{ave}) was calculated using equation 8. From the average strain the circumferential thrust force within the culvert was then calculated using the culvert's axial stiffness (EA) using equation 9.

$$\varepsilon_{ave} = \varepsilon_1 - \left(\frac{h+t}{2h}\right)(\varepsilon_1 - \varepsilon_2) \quad (8)$$

$$N = \varepsilon_{ave} EA \quad (9)$$

ε_{ave} is average strain, ε_1 is the strain on the inner corrugation valley on the inside surface of the culvert, ε_2 is the strain on the outer corrugation crest on the inside surface of the culvert, h is radial distance between gauges (mm) = 25.4 mm, t is the wall thickness (mm), N is the thrust force per unit length (kN/m), E is the Young's modulus (MPa), and A is cross sectional area of wall per unit length (mm^2/m).

The curvature was calculated using the measured strains such that a positive curvature would produce tensile strains on the outer surface and compressive strains on the inner surface of the culvert. Curvatures and bending moments were calculated from equations 10 and 11, respectively.

$$\kappa = \frac{\varepsilon_2 - \varepsilon_1}{h} \quad (10)$$

$$M = EI\kappa \times 10^{-3} \quad (11)$$

κ is the curvature (10^{-6}/mm), M is the bending moment (kNm/m), and I is the second moment of area per unit length (mm^4/mm)

Results and Discussion

Response due to backfilling

The vertical and horizontal diameter changes of the ellipse with increasing backfill height (the height of the soil above the base) were plotted in Fig. 4. At a backfill height of 1.35 m (top of crown), the ellipse experienced a vertical diameter change of 0.9 mm (crown moving upwards) and horizontal diameter change of -1.1 mm (springlines – sides of the pipe – moving inwards). Once the backfill height rose above the crown, the culvert started to contract in the vertical direction and expand in the horizontal direction. Upon completion of backfilling, the culvert had contracted 2.1 mm in the vertical direction and expanded 0.8 mm in the horizontal direction. For a circular culvert, the expectation is that the vertical and horizontal diameter changes due to backfilling would be equal but opposite, but this was not the case here. The larger vertical diameter change compared to the horizontal diameter change was believed to be due to the elliptical shape of the culvert. The radius of the crown and invert was much larger than the radius of the springlines, which resulted in the culvert being less stiff in the direction of vertical loading enabling larger diameter changes in the that vertical direction.

The circumferential thrust forces and bending moments in the culvert due to backfill are presented in Fig. 5(a) and (b), respectively. The stress resultants for the ellipse, a non-circular culvert, were plotted on a polar plot. Thus, the culvert's shoulders (midway between the side and the top of the pipe) and haunches were not in the same position they would be for a circular pipe but were closer to the springlines in the plot. Fig. 5(a) illustrates that the thrust force was compressive from the crown to the springlines, and below the springlines the thrust force decreases to approximately zero at the invert. The bending moments in Fig. 5(b) at both the crown and springlines were approximately zero, which when considered in conjunction with the

axial forces suggested that this elliptical culvert was behaving in a similar fashion to a circular pipe during backfilling. Bending moments developed at the invert and haunches, which was likely a function of the hard bedding directly at the invert coupled with soil that was less well compacted under the haunches (due to limited access). Thus, the culvert was likely experiencing load concentrations at the invert that resulted in localized bending moments.

Response due to live loading – Service load response

For the service load tests, the load was cycled between zero applied load and the maximum service load three times. The results reported here are for the third load cycle unless otherwise indicated. The third load cycle is used because the first load cycle causes further compaction of soil in the system and so is not representative of the typical response of the culvert to loading. Removing these initial effects allows the results to be more realistically compared to the response of structures in the field and numerical models in the future. The second and third load cycles typically yield almost the same results. Some permanent deformation will have occurred as the culvert is buried to 0.9m, subjected to load cycles, and half of that overburden is then removed. However, the incremental response reported during the third loading cycle at 0.45m of cover is largely elastic, and so is not expected to have been significantly influenced by the earlier loading history.

Under service loading at 0.9 m of cover, the diameter changed a total of –4.5 mm in the vertical direction and 2.9 mm in the horizontal direction at 0.9 m of cover. At 0.45 m of cover, the diameter changed a total of -3.9 mm in the vertical direction and 2.9 mm in the horizontal direction. The diameter change results indicated that the culvert experienced a greater diameter change under service loading at 0.9 m of cover. The deflected shapes for the culvert at 0.9 m and

0.45 m of cover are presented in Fig. 6(a) and (b), respectively. These deflection results were taken at the North location, which was the critical location directly underneath two of the wheel pads. The deflected shapes for the two burial depths showed two different behaviors. At 0.9 m of cover, the culvert's deflected shape had the greatest deflections at the crown, and overall the shape demonstrated typical ovaling behavior. The deflected shape at 0.45 m of cover, on the other hand, showed that the greatest deformation within the culvert was at the shoulders. This difference in deflected shapes was related to the cover depth, since at 0.9 m of cover the load was able to be spread through the soil to a greater degree, so the culvert experienced a more uniform vertical load. However, at 0.45 m of cover there was reduced load spreading, and the maximum loading points were directly below the wheel pads, so the largest deflection occurred at the shoulders. Therefore, although the magnitude of the diameter changes under service loads were similar at the two cover depths, restriction of deflections to the shoulders of the shallow buried pipe resulted in deflected shapes at the two burial depths that were very different.

Fig. 7 and 8 show the circumferential thrust forces and bending moments for the service load applied at each burial depth (0.9 m and 0.45 m). In Fig. 7(a), the maximum thrust forces at 0.9 m of cover were seen to be at the North location and the thrust was evenly distributed around the top half of the culvert. In Fig. 7(b), the thrust forces at 0.45 m of cover had a different distribution with the largest thrusts concentrated at the crown and springlines, with small values of thrust at the shoulders and below the springlines. This suggests that the culvert was behaving in ring compression at 0.9 m of cover but not at 0.45 m of cover. This observation correlated well with the earlier observation about the difference in deflected shapes at the two burial depths.

The bending moment plots under service loading conditions for 0.9 m of cover are given in Fig. 8(a), and for 0.45m of cover in Fig. 8(b). These also indicate that the culvert behavior is

different at the two cover depths. At 0.9 m of cover, the peak bending moments were at the crown, invert and springlines as one would expect for typical ovaling behavior. However, at 0.45 m of cover, significant bending moments developed at the springlines, shoulders and crown indicating that the top of the culvert is no longer acting in pure ring compression. This bending behavior matched the deflected shape (Fig. 6(b)) and suggests that as the cover depth was decreased, a greater amount of load was being transferred directly to the culvert and was changing the culvert's load carrying mechanism from thrust to flexure. Given that the flexural stiffness of these structures is relatively low compared to their axial (i.e. hoop) stiffness, this change in behavior should result in a lower ultimate limit state response at this cover.

Response due to live loading – Ultimate limit state testing

Two ULS tests were conducted: U1 and U2. After reaching a total force of 950 kN during the U1 test it was observed that the West wheel pads were experiencing more bearing failure than the East wheel pads. Since uneven bearing failure meant that there was rotation and sway in the actuator and loading pads, the culvert was unloaded. The ground surface was then repaired and re-compacted to a density of 95% standard Proctor, before the culvert was retested to its ULS in test U2.

In Fig. 9, the load deflection plots for both ULS tests (U1 and U2) are presented. They show the vertical diameter changes at the North location for both ULS tests against their respective applied loads. The ellipse had a higher initial stiffness until approximately 400 kN where its curve became non-linear in test U1 whereas, in test U2 the ellipse had a lower initial stiffness but remained linear until approximately 700 kN, and remained almost linear until the load exceeded 900kN. The lower stiffness in test U2 was believed to be due to non-symmetric

loading of the culvert in test U1 causing permanent deformations and localized damage to the culvert structure. The deflected shape of the ellipse at 950 kN (maximum loaded achieved during test U1) in Fig. 10 illustrated that the culvert was deforming locally in test U1 at this load due to the asymmetric loading. This lends credence to the assumption that the lower stiffness in test U2 was due to the local damage. It is not possible to quantify the impact that test U1 had on the response of the specimen during test U2 in terms of both its stiffness and ultimate capacity. However, while this damage appears to have had some effect on the stiffness in test U2, the culvert response was linear with load until a much higher load (700 kN versus 400 kN), and its ultimate load was higher still. Therefore, the impact of U1 on the ultimate capacity was likely modest. During the U2 ULS test, the ellipse was first loaded to its fully factored load of 624 kN, where it contracted 7.3 mm vertically and expanded 5.8 mm horizontally. It was then loaded in 50 kN increments until the culvert failed. At approximately 1324 kN, there was a significant bearing failure on the surface (approximately 26 mm in depth), which was attributed to the failure of the culvert at the West shoulder. Fig. 11 shows the localized three hinge plastic collapse mechanism that formed at 1324 kN.

The thrust force and bending moment plots described below are only presented for the North location as it was the most critical location in terms of these values. The circumferential thrust forces and bending moments calculated using the measured strains for the ellipse at 624 kN (the fully factored load) and 1300 kN (just prior to the ultimate load) are presented in Fig. 12(a) and 12(b), respectively. At 624 kN the maximum thrust force was -136 kN/m at the West springline and at 1300 kN the maximum thrust force was -392 kN/m also at the West springline. At both loads, the thrust forces between the 4 o'clock and 8 o'clock positions below the springlines were approximately zero. However, there was a distinct difference in the distribution

of the thrust forces at 624 kN versus 1300 kN. At 624 kN, the culvert was largely in ring compression with the thrust force reducing locally at the shoulders. This observed behavior correlated with the load deflection response where there was not a significant change in stiffness until after 700 kN for test U2. At 1300 kN, the thrust forces were much more variable indicating that the culvert is no longer carrying the applied load in ring compression.

The bending moments within the ellipse shown in Fig. 12(b) also illustrate this change in behavior between the fully factored and ultimate loads. At both 624 kN and 1300 kN, the moments were positive at the shoulders and negative at the crown and springlines with the bending moments at the invert resulting from the variable stiffness of the soil support as discussed earlier. From Fig. 12(b) it was also seen that the moments at the West shoulder were approaching the yield moment at an applied load of 624 kN, indicating that the culvert was about to develop a plastic hinge at this location. As noted previously the presence of thrust reduces the moment required to produce yield. However, as can be seen in Fig. 12(a), the thrust force in the location of the maximum moments is essentially zero meaning that using the yield moment calculated without thrust is reasonable. Once again, this result matched well with the observation that the culvert's stiffness changed at 700 kN, suggesting that this change in stiffness was due to the formation of plastic hinges. At 1300 kN, the moments at both the shoulders and springlines exceed the yield moment although the moments in Fig. 12(b) were calculated assuming elastic behavior and so are not correct above the yield moment, but instead serve to illustrate that the yield moment was exceeded and plastic hinges started to develop.

Failure mode

According to the Handbook of Steel Drainage & Highway Construction Products (CSPI, 2009), corrugated steel culverts are designed based on compression failures due to wall crushing or buckling. The effect of local bending moments and the potential development of plastic hinges are usually disregarded under service loading. The handbook predicts the failure mechanism of a culvert with a span of less than 3 m based on the ratio of the diameter (D) to the radius of gyration (r). The radius of gyration for the ellipse was 8.685 mm, resulting in a D/r ratio of 184.25. Therefore the governing failure mechanism outlined for this culvert with $D/r < 294$ by the handbook was yielding of the culvert wall. The maximum thrust force at 1300 kN was -392 kN/m located at the West springline of the culvert, which was approximately 80 % of the culvert's compressive yield strength. But at 1300 kN the culvert had already yielded in bending at both shoulders, both springlines, and the crown. Therefore, these results suggest that current design methods might be using the wrong failure mode for this particular geometry, cover depth and loading type. The previous loading history during backfilling, service load testing with removal of half of the overburden, and during the first ULS test, produced residual displacements and stresses in the pipe and the surrounding soil. Thus it is unclear whether the final deformations and stresses in the culvert would have been the same if the load history was changed (e.g. if it was buried and immediately loaded to failure). However, the test culvert had more than sufficient strength, with capacity more than double the fully factored load. Furthermore, culverts in the field can be expected to experience even more complex loading histories during construction and in service.

Comparison to Design Codes

The AASHTO (2007) (equation 1) and Canadian (CSA, 2014) (equations 2 through 5) design procedures were used to estimate the total thrust force in the structure and the results of this analysis are given in Table 2.

At 0.9 m of cover, the Canadian code provides an estimate of the thrust (22.4 kN/m) that falls in between the two values measured at the springlines (21 and 27 kN/m). However, it underestimates the maximum thrust in the culvert (30 kN/m) which occurs at the shoulder. The AASHTO estimate of 32.1 kN/m is within 10% of the maximum thrust but overestimates the springline thrusts. The impact of bending on the culvert behavior at this cover seemed to be minimal based on the diameter change and strain measurements and so these results suggest that the AASHTO code may provide the superior estimate of maximum thrust force at this cover. However, both codes are based on the assumption that the maximum thrust occurs at the springline, which was not the case.

At 0.45 m of cover, the Canadian code estimate of thrust (40.0 kN/m) again lay between the experimental values at the springlines (36 and 51 kN/m) suggesting that it is providing an effective estimate of springline thrust. The AASHTO estimate (51.1 kN/m) is in excellent agreement with the maximum measured thrust at the springline (51 kN/m). Both codes underestimate the maximum thrust of 102 kN/m, which was observed at the crown. However, this is to be expected, since both design procedures trace their origins to ring compression theory (White and Layer, 1960) where thrust dominates, whereas the experimental results indicate that significant bending developed across the top of the culvert at this cover depth.

The Canadian code also enables the bending moment in the culvert during construction to be estimated using equation 7. The maximum moment in the culvert at 0.45 m of cover was observed (calculated from measured strains) to be 1.35 kN/m at the West Shoulder, while the

Canadian code provided an estimate of maximum moment of 2.0 kN/m. The code estimate is of the correct order of magnitude, though it is 50% conservative, whereas the maximum thrust force obtained using the Canadian procedure at this cover depth was 60% too low. Therefore, while the Canadian code allows the designer to consider bending moments (unlike the AASHTO design procedure), these moment estimates may be considered to be over-conservative for this particular structure. These results indicate that a more refined computer analysis procedure for the design of these structures may be required. However, those procedures need to account for the stiffness of the soil, the flexural stiffness of the culvert, the geometry of the culvert (i.e. span and initial curvature), and the three dimensional nature of the overlying vehicle load (e.g. Elshimi et al., 2014). The experimental results presented here can be used to develop improved analyses, and laboratory testing of culverts with other geometries to expand the database of results would also be valuable.

Conclusions

The objectives of this research program were to (i) investigate the behavior of a horizontal ellipse culvert during backfilling, (ii) examine the failure mode of a horizontal ellipse culvert and, (iii) assess the overall stability of this type of culvert. The following key conclusions were drawn from this research:

- This horizontal ellipse culvert behaved in a manner similar to a circular culvert during backfilling, although the vertical diameter change was larger than the horizontal diameter change, reflecting that the vertical stiffness is lower than the horizontal stiffness for a horizontal ellipse.

- At 0.9 m of cover with adequate surrounding soil compaction, the culvert tested appeared to carry the load in ring compression as would be assumed by design procedures used for these structures.
- Load history (e.g. the irrecoverable deformations after the first service cycle) could potentially affect the behavior of the culvert during later tests. However the incremental responses that have been reported are believed to be largely indicative of the elastic culvert behavior, regardless of the history or prior loading.
- At 0.45 m of cover, the behavior of the culvert changed and localized bending across the top half of the structure started to appear as the dominant load carrying mechanism.
- At a load of approximately 1300 kN, the culvert developed 5 plastic hinges and was no longer experiencing uniform ring compression; it did not develop the failure mechanism considered by the existing design models for structures of this type.
- At the ultimate load of 1324 kN, the structure failed due to the formation of a three hinge plastic collapse mechanism across one shoulder.
- Although this culvert did not fail in the expected manner, the culvert was able to withstand approximately twice the fully factored load. A potential new design model based on combined thrust and bending mechanism, similar to the construction load limit state considered in the Canadian code, could be used to account for the observed behavior. However, such an approach would require careful consideration of a number of parameters including soil stiffness, culvert flexural stiffness, and culvert geometry, and thus a more extensive experimental database would be valuable for robust model development.

Acknowledgements

The authors wish to thank the Natural Sciences and Engineering Research Council of Canada, the Canada Foundation for Innovation, and the Ministry of Research and Innovation Ontario for their generous financial support of this research. The authors would also like to thank Graeme Boyd, Jacob Tetreault and Brian Westervelt for their excellent assistance.

References

AASHTO. (2007). "AASHTO LRFD bridge design specifications, SI Units, 4th edition." Washington, DC.

American Society for Testing and Materials (ASTM), (2015). *A796/A796M - Structural Design of Corrugated Steel Pipe, Pipe-Arches, and Arches for Storm and Sanitary Sewers and Other Buried Applications,* ASTM, West Conshohocken, PA.

Canadian Standards Association (CSA), (2014). *CAN/CSA-S6-14 – Canadian Highway Bridge Design Code,* CSA, Mississauga, ON.

Corrugated Steel Pipe Institute (CSPI). (2009). *Handbook of Steel Drainage & Highway Construction Products - Second Edition,* CSPI, Cambridge, ON.

Duncan, J. M. (1978). “Soil-Culvert Interaction Method for Design of Metal Culverts.” *Transportation Research Record* 678, Washington, DC, TRB, National Research Council pp. 53–58.

Duncan, J.M., Seed, R.B. and Drawsky, R.H. (1985). “Design of Corrugated Metal Box culvert”. *Transportation Research Record* 1008, 1985.

El-Sawy, K.M. (2003). “Three-dimensional modeling of soil-steel culverts under the effect of truckloads.” Thin-walled structures, 41(8), 747-768.

Elshimi, T., Brachman, R.W.I. and Moore, I.D. (2014). “Effect of truck position and multiple truck loading on response of long-span metal culverts.” *Canadian Geotechnical Journal*, 51(2), 196-207.

Lougheed, A.C. (2008). *Limit States Testing of a Buried Deep-Corrugated Large-Span Box Culvert*. MSc Thesis, Department of Civil Engineering, Queen’s University, Kingston, Canada.

Mai, V. T., Hoult, N. A., and Moore, I. D. (2013). “Effect of deterioration on the performance of corrugated steel culverts.” J. Geotech. Geoenviron. Eng., 10.1061/(ASCE)GT.1943-5606.0001021, 04013007.

Mirza, C. and Porter, W. A. (1981). “Construction considerations and controls for soil-steel bridge structures.” *Canadian Journal of Civil Engineering*, 8(4), 519-534.

Moore, I. D. (1988a). “Elastic stability of buried elliptical tubes.” *Geotechnique*, 38(4), 613-618.

Moore, I. D. (1988b). “Static response of deeply buried elliptical tubes.” *Journal of Geotechnical Engineering*, 114(6), 672-687.

Moore, I. D. (2012). “Large-scale laboratory experiments to advance the design and performance of buried pipe infrastructure.” 3rd Int. Conf. on Pipelines and Trenchless Technology, ASCE, Reston, VA, 805–815.

Moore, R. G., Bedell, P. R., and Moore, I. D. (1995). “Investigation and assessment of long-span corrugated steel plate culverts.” *Journal of Performance of Constructed Facilities, 9*(2), 85-102.

Seed, R.B. and Raines, J.R. (1988). “Failure of Flexible Long-span Culverts under Exceptional Live Loads.” Transportation Research Record, 1191, 22-29.

Simpson, B., Hoult, N., and Moore, I. (2015). “Distributed Sensing of Circumferential Strain Using Fiber Optics during Full-Scale Buried Pipe Experiments.” J. Pipeline Syst. Eng. Pract. , 10.1061/(ASCE)PS.1949-1204.0000197 , 04015002.

Take, W.A. (2015). “Thirty-Sixth Canadian Geotechnical Colloquium: Advances in visualization of geotechnical processes through digital image correlation.” *Canadian Geotechnical Journal*, 52(9): 1199-1220, 10.1139/cgj-2014-0080.

Taleb, B. and Moore, I. (1999). “Metal culvert response to earth loading: Performance of two-dimensional analysis.” Transportation Research Record, 1656, 25-36.

White, H. L. and Layer, J. P. (1960). “The corrugated metal conduit as a compression ring.” *Highway Research Board Proceedings*, 39, 389-397.

528 **Table 1. Summary of backfill properties**

Soil Location	Dry Density (g/cm^3)	Water Content (%)	Standard Proctor (%)
Bedding	2.2	3.6	96.4
Invert to Crown	2.1	4.0	92.6
Crown to top of 900 mm Cover	2.2	4.8	95.6
Crown to top of 450 mm Cover	2.2	4.7	96.3

529

530 **Table 2. Comparison of experimental and code estimated thrust values**

Cover	Experimental Results		Code Estimates	
	Location	Thrust (kN/m)	AASHTO (kN/m)	CSA (kN/m)
0.9	W. Shoulder	30	32.1	22.4
	W. Springline	21		
	E. Springline	27		
	Crown	18		
0.45	W. Springline	102	51.1	40
	E. Springline	36		
	Crown	51		

531

List of Figures

Fig. 1. Culvert specimen: (a) aligned in the trench before burial in the testing pit, (b) after burial under the tandem axle loading frame

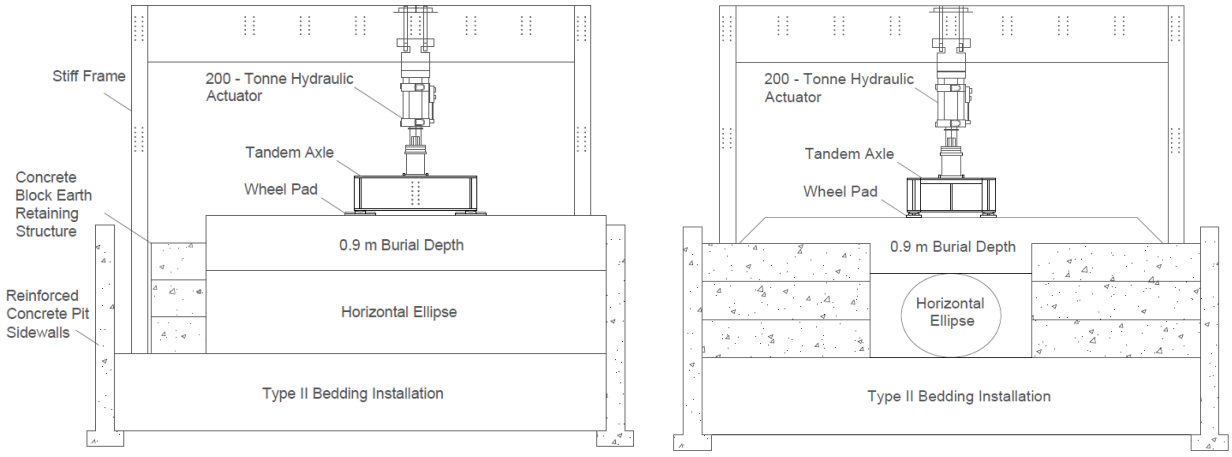

Fig. 2. Side profile of test pit showing location of the test specimen in the 0.9 m cover configuration: (a) West profile of test pit, (b)North profile of test pit

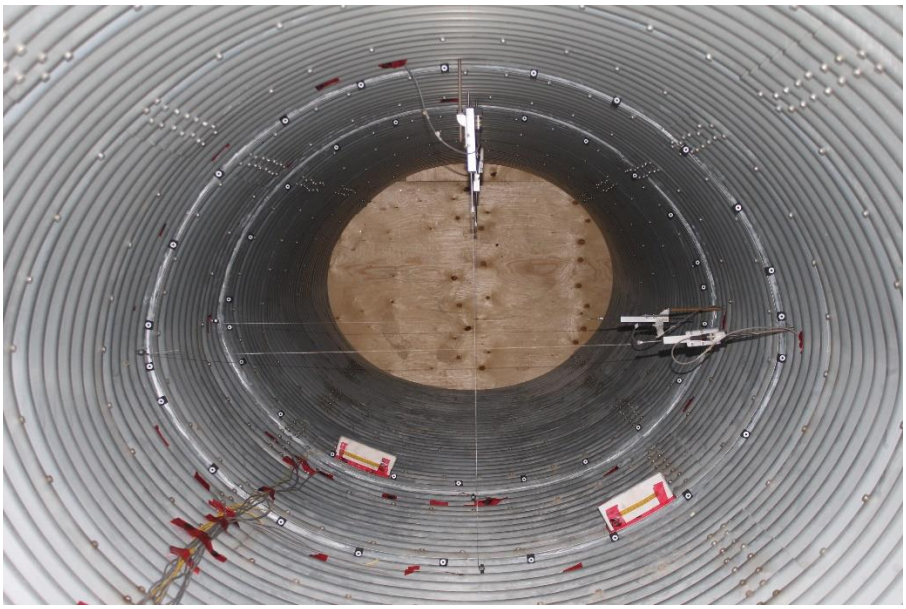

Fig. 3. Image of the culvert used for the DIC analysis showing the locations of the linear potentiometers, the DIC targets, and the fiber optic sensor cables

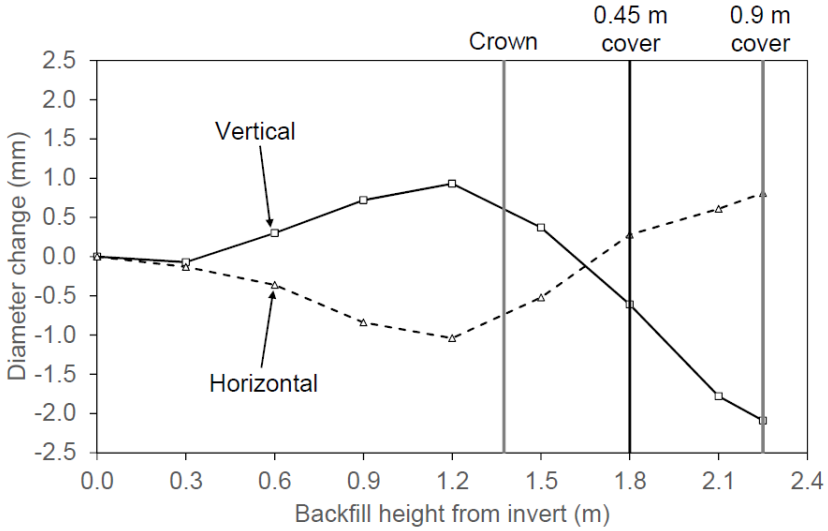

Fig. 4. Vertical and horizontal diameter change with increasing backfill height

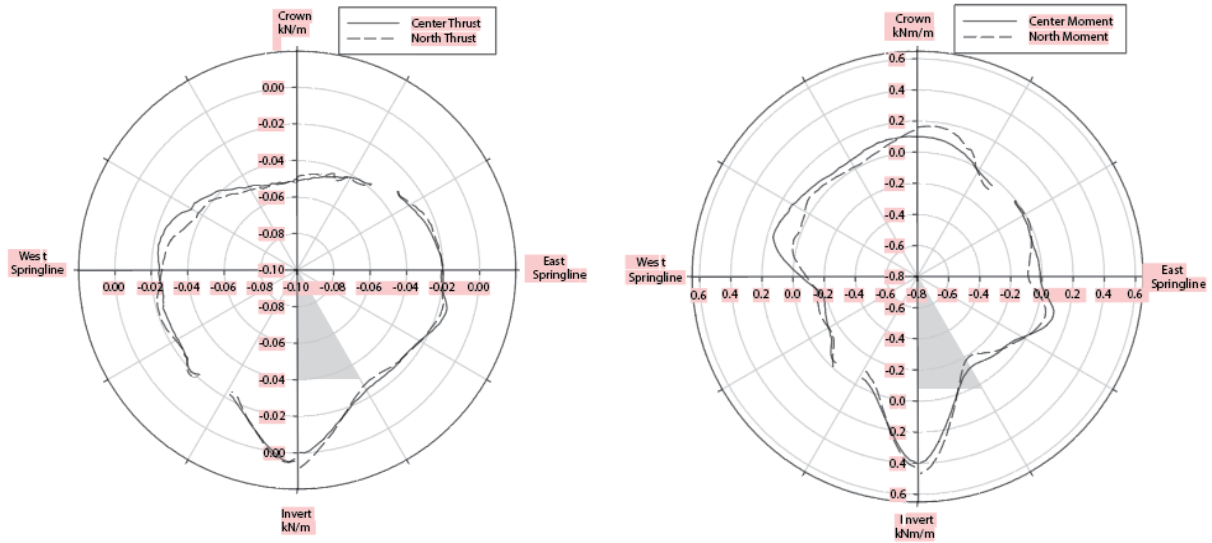

Fig. 5. Circumferential response of the specimen due to backfilling: (a) Thrust forces, (b) Bending moments

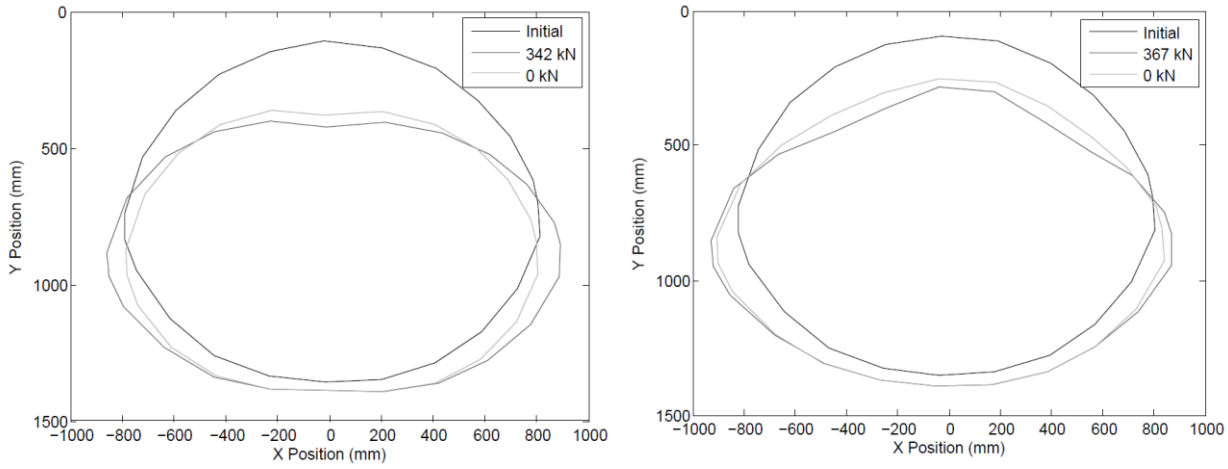

Fig. 6. Deflected shape of specimen due to service load at different cover depths also showing permanent deformations at 0 kN (Note: the deflection results have been multiplied by a factor of 50 for clarity): (a) Cover depth of 0.9 m, (b) Cover depth of 0.45 m

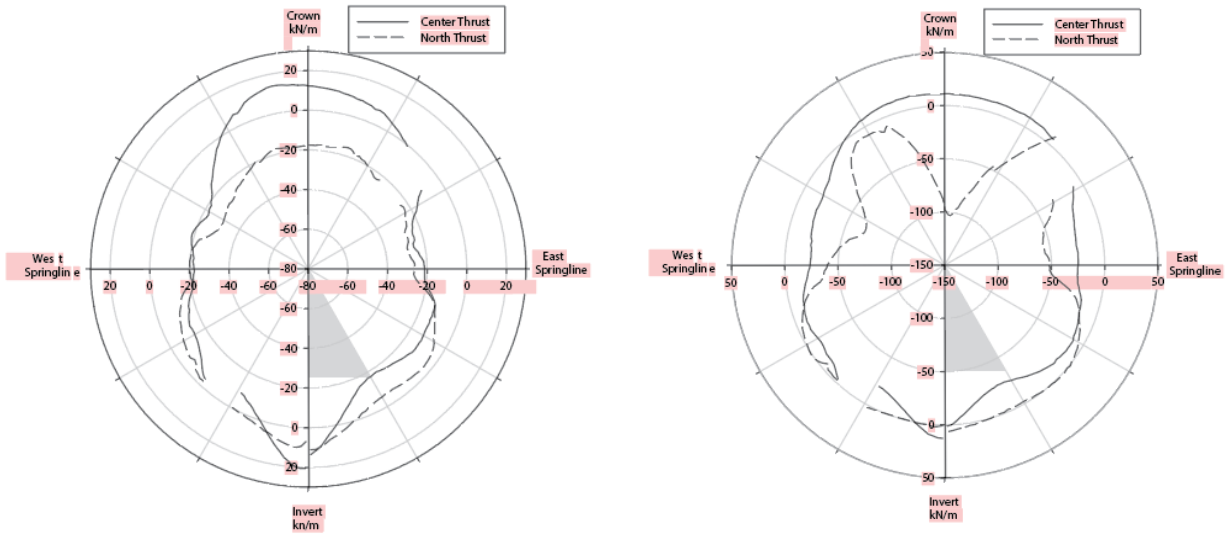

551

552 Fig. 7. Thrust forces around the circumference of the culvert due to service load at different

553 cover depths: (a) Cover depth of 0.9 m with applied surface load of 342 kN, (b) Cover depth of

554 0.45 m with applied surface load of 367 kN

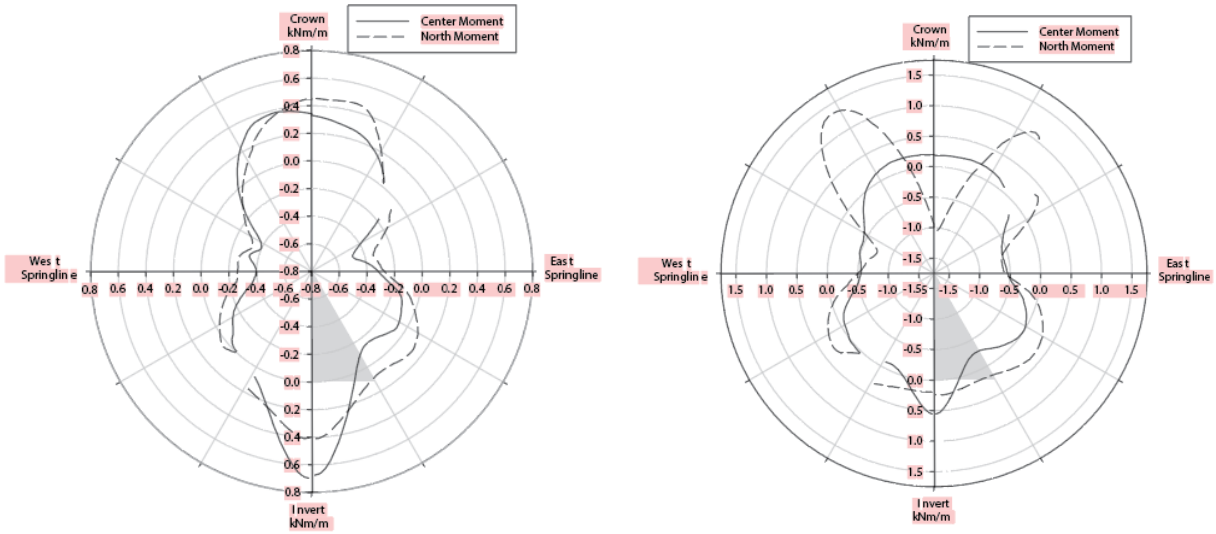

555

556 Fig. 8. Bending moments around the circumference of the culvert due to service load at different

557 cover depths: (a) Cover depth of 0.9 m with applied surface load of 342 kN, (b) Cover depth of

558 0.45 m with applied surface load of 367 kN

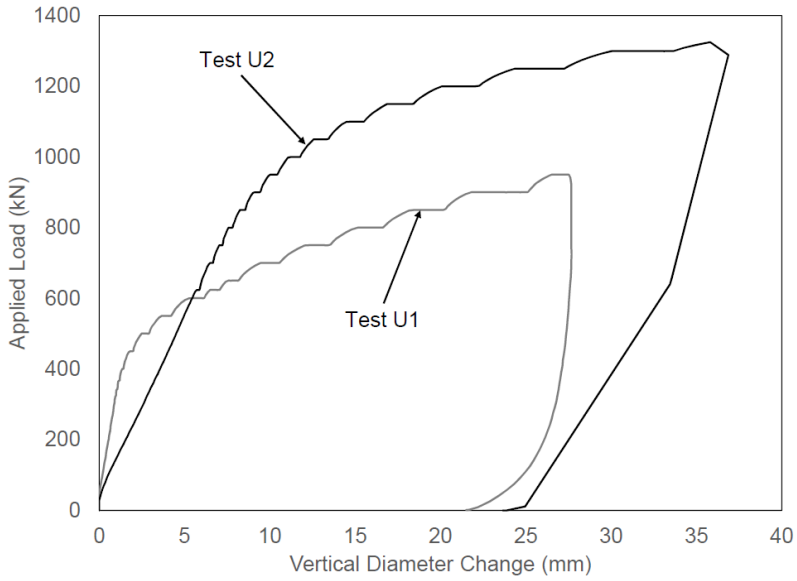

559

560 Fig. 9. Load versus vertical diameter change for both U1 and U2 tests

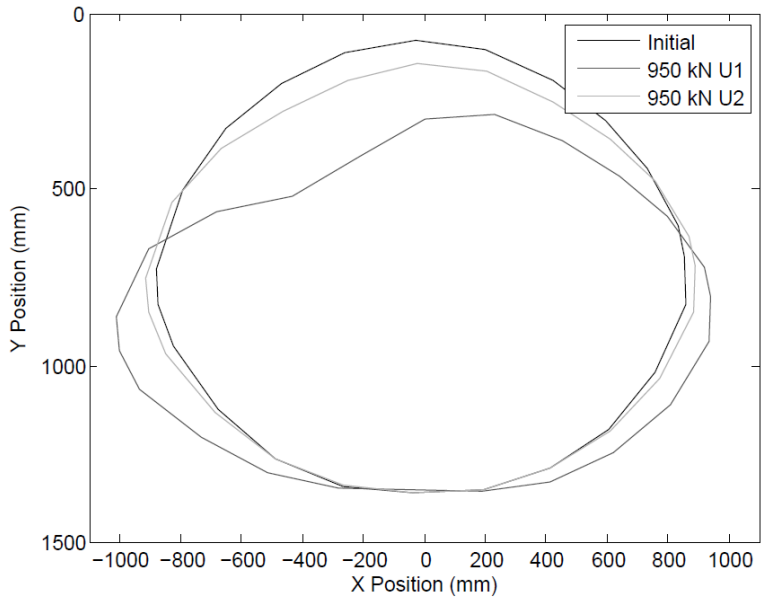

561

562 Fig. 10. Deflected shape of the ellipse during both ULS tests (U1 and U2) at 0.45 m of cover

563 showing the non-symmetrical deflected shape that occurred during test U1 (Note: the deflection

564 results have been multiplied by a factor of 10 for clarity)

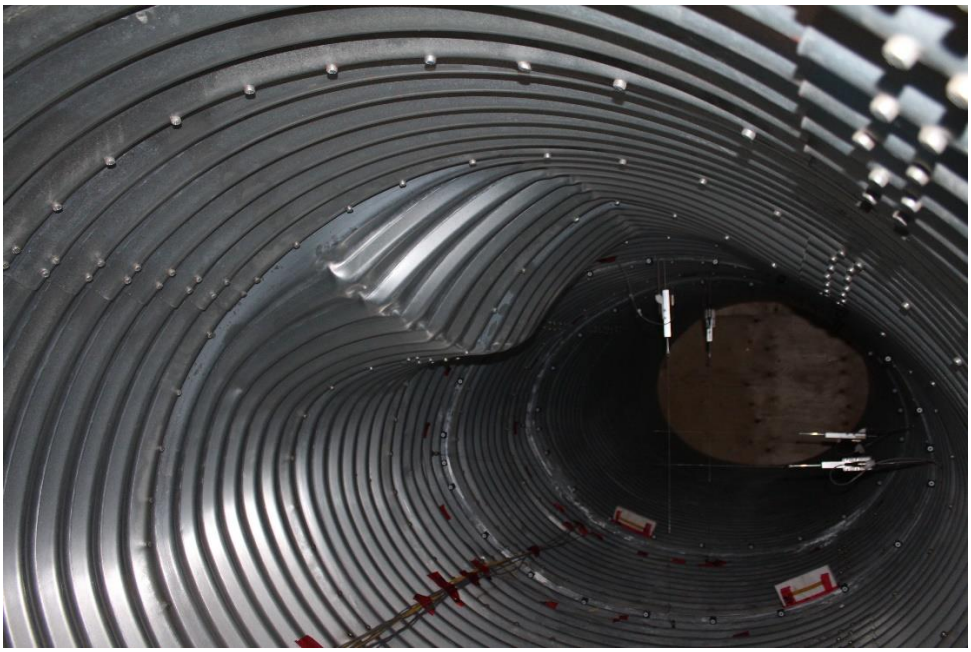

Fig. 11. Localized bending failure of the culvert with a three hinge plastic collapse mechanism visible

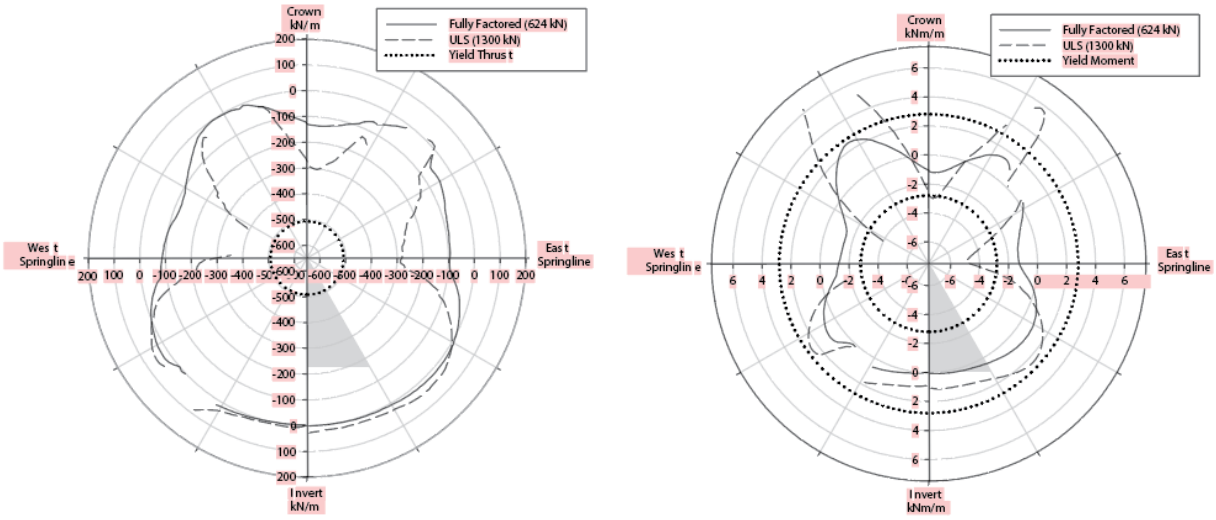

Fig. 12. Circumferential structural response of the specimen during the ULS test: (a) Thrust forces at the fully factored (624 kN) and near the ultimate loads (1300 kN), (b) Bending moments at the fully factored and near the ultimate loads